A LABORATORY ANALOGUE MODEL STUDY OF MAGNETIC VARIATIONS INDUCED BY OCEAN WAVES

by

TIMOTHY JOHN MILES

B.Sc., University of Victoria, 1976

A THESIS SUBMITTED IN PARTIAL FULFILLMENT
OF THE REQUIREMENTS FOR THE DEGREE OF
MASTER OF SCIENCE
in the Department
of
Physics

ACCEPTED
FACULTY OF GRADUATE STUDIES
[redacted]
DEAN
DATE 16th Apr 78

We accept this thesis as conforming
to the required standard

[redacted]

Supervisor: Dr. H. W. Dosso

ABSTRACT

This thesis deals with a laboratory analogue model study of the horizontal component of the magnetic field induced by ocean waves. Following some of the techniques proposed by Ng and Dosso (1970), an analogue model, employing mercury to simulate the ocean, was constructed. The validity of this model was tested by comparing the observed model magnetic field with the magnetic field calculated using Podney's (1975) expression for a finite uniform depth ocean. Excellent agreement was obtained.

The model was used to study cases of non-uniform ocean depths and sea-land interfaces. Measurements of the induced magnetic field were carried out for traverses over a (i) uniform depth model (to provide a reference), followed by various ocean floor and coastline structures, that is, the (ii) step and shelf model, the (iii) wedge and shelf model, the (iv) dyke model, the (v) sea mount model, the (vi) sloping bay and shelf model, and the (vii) reef and shelf model. For shallow ocean depths, over a submerged obstacle (or structure) of large horizontal extent, the attenuation of the induced horizontal magnetic field over the leading edge of the structure is strongly dependent on the depth. The shape of the leading edge of the structure can also have an important effect (especially for the very shallow fluid depths), this being brought out for the models having vertical and sloping sea-land interfaces.

The contour of the coastline affects the induced field through changes in the fluid waves or changes in the electric currents induced by the waves. The observed fields for the bay model are attributed to the focussing of the fluid waves by the geometry of the bay, while the observed fields for the reef model are in agreement with channelling of induced currents around the reef, since the reef was parallel to the direction of wave propagation. The horizontal extent of the structure is important, since fluid wave interference effects would be expected. For the case of the dyke model, and also for the case of the sea mount model, the horizontal extent is approximately half a wavelength in the direction of wave propagation, and constructive interference occurs resulting in large enhancements of the induced field over the trailing edges of the horizontal section for both the dyke and sea mount models. In general, it is apparent that an irregular ocean bottom, or a large submerged structure, affects the induced fields at the surface only for rather shallow ocean depths (less than 40 m for a wavelength of approximately 360 m). Thus it appears that it may be feasible to use aerial measurements of ocean wave induced magnetic fields to detect shallow structures such as reefs and sea mounts.

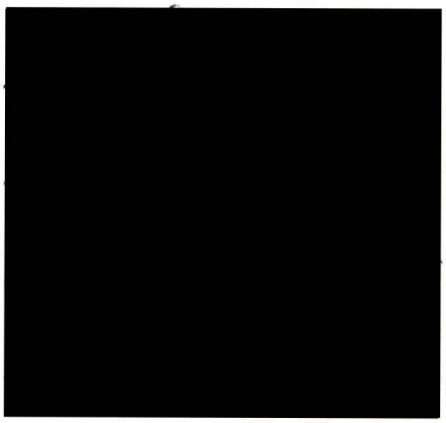

TABLE OF CONTENTS

LIST OF TABLES

LIST OF FIGURES

ACKNOWLEDGEMENTS

I would like to thank my supervisor, Professor H. W. Dosso, for his suggestion of the thesis topic, and for providing guidance and financial support throughout this research. As well as kindly offering his time and careful attention, Dr. Dosso's persistent interest in this research has been a tremendous source of inspiration.

I would also like to take this opportunity to thank Mr. G. H. Chan, Dr. J. P. Elliott, Mr. V. R. Green, Dr. R. Hibbs, Mr. W. Nienaber, and Dr. J. T. weaver, all from the University of Victoria, and Dr. S. Ogunade, now from the University of Ife, Nigeria for their helpful comments, constructive criticisms, and suggestions, as well as Mr. E. Chan from the University of Victoria, for his help in carrying out the model measurements. Financial assistance from the University of Victoria is gratefully acknowledged.

CHAPTER 1

INTRODUCTION

1.1 Historical Review

The geophysical interest in magnetism was a direct consequence of sailors' desire to navigate beyond sight of the horizon. The compass was known in Europe, as concluded from the records of the monk Alexander Neckham (1163) of St. Albans, England. It became apparent that the compass did not always point to true north. Sundials dating from 1450 show a correction for the magnetic declination, and the magnetic dip was mentioned in a Nuremberg letter of date 1544.

From a rudimentary knowledge of the magnetic dip and declination, the science of geomagnetism evolved. Gilbert (1600), in his famous book 'De Magnete', expressed his belief that the earth itself was a giant magnet. His contemporary, Gellibrand, in 1635 demonstrated that the magnetic properties of the earth changed with time, at a rate too rapid to be considered on a geological time scale. From this began the study of the secular, or long term variations of the earth's field.

On a shorter time scale, transient geomagnetic variations were noted by Graham in 1724, as he examined the movements of a compass needle under a microscope. His contemporary Celcius began simultaneous observations in Uppsala, and the two geophysicists exchanged data. The global nature of geomagnetic variations soon became apparent, and the correlation between magnetic disturbances and aurora was noted by Celcius in 1741.

The theoretical basis for geomagnetic induction was laid by Faraday, in the year 1832. He noted that a time varying magnetic field generated an electric current in a conductor. On a geophysical scale, these currents were noted by Barlow (1849) in a paper to the Royal Society entitled 'On The Spontaneous Electric Currents Observed In The Wires Of The Electric Telegraph'. Scientific field stations were set up in 1865 to record these currents.

Not only can a time varying magnetic field induce a current flow, but also a conductor, moving in a magnetic field. Faraday, in a lecture in 1832, pointed out that water, moving in the earth's magnetic field, should generate an electromotive force. He attempted to measure the voltage induced across the river Thames with a station

at Waterloo Bridge, but the results were inconclusive.

One of the earliest successful attempts to measure induced current flow was carried out by the British and described in a paper by Young et al (1920). The induced electric field was successfully measured outside Dartmouth Harbour, and strong evidence of current flow was found, consistent with the hypothesis of electric fields induced by tides. Towed electrodes were also used to measure the induced field due to the motion of a ship. In all cases, the electric field obtained was shown to be consistent with Faraday's theory, and the field from towed electrodes showed evidence of induction by wave action. The field induced by waves was found to be maximized in a direction normal to wave propagation, and this was consistent with Maxwell's equations.

A theoretical study of the electric field induced by ocean waves was carried out by Longuet-Higgins et al (1954), and the results showed that the effect of the ocean bottom was negligeable for ocean depths comparable to the English Channel. This study divided each wave into infinitesimal 'streams', with the velocity of fluid particles in each stream being a constant at any given time. The total current induced by the wave was then calculated by summing over the contributions from each

infinitesimal stream. This procedure was placed on a firm theoretical basis by Crews and Futterman (1962), who calculated the magnetic field produced by these induced currents.

1.2 Magnetic Fields Induced by Ocean Waves

Exact theoretical analysis of the magnetic field associated with ocean waves and swell can be said to date from Warburton and Caminiti (1964). They used the current strip approach, developed by Crews and Futterman (1962) to obtain integrals giving the magnetic field induced by ocean waves, directly without solving for the induced currents. These integral expressions were evaluated numerically for the various field components, and graphs were presented showing the effect of the magnetic declination and magnetic dip upon the field.

Weaver (1965) presented an elegant solution for the magnetic fields induced by waves in an ocean of infinite depth. In Weaver's (1965) approach, Maxwell's equations, the Lorentz equation, and the fluid equation giving particle velocity, were combined to produce a second order differential equation, giving the magnetic field as a function of position. Two of the more important properties that

followed from his investigations were:

1. The intensity of the field decays exponentially with altitude if the ocean is uniform and isotropic. (The decay constant is the wave number.)

2. The intensity of the field is a linear function of the wave amplitude, and almost a linear function of the wave length. The second prediction agreed well with the earlier observations of Maclure et al (1964), who used a rubidium vapour magnetometer anchored at various depths in the ocean.

Woods (1965) and Groskaya (1972) obtained solutions for the case of the field induced over an ocean of finite depth, assuming irrotational motion of the fluid elements. This work was then generalized by many authors, including Podney (1975), who treated the general case of induction in oceans of finite depth, without the assumption of irrotational motion. Beal and Weaver (1970) calculated the magnetic field induced by internal ocean waves, while Larsen (1971) treated the problem of a plane progressive wave moving through an ocean of uniform depth, assuming uniformly conducting layers that represented the ocean, the bottom sediments, the crust, and the mantle.

Preisendorfer et al (1974) provided an exhaustive theoretical study of the magnetic field induced by both surface and internal ocean waves. In this study, the ocean waves were treated as antennae producing magnetic fields, and a multi-layered ocean bottom was treated as a series of leaky waveguides through which these magnetic fields propagated. Various modes of electromagnetic wave propagation were numerically shown to exist in the ocean floor, and graphs of these modes were presented. Klein et al (1975) carried out simultaneous measurements of the vertical and horizontal magnetic field components induced by ocean swell for the period range of from one to two hundred seconds. They mentioned the possibility of utilizing the induced field to determine inhomogeneities in the underlying geological structure. Such a survey of the geological structure would require precise knowledge of the effect on the induced field from various common geological structures.

Much of the work in the field of magnetic induction by ocean waves has assumed horizontal symmetry. An

exception to this is the work of Leibo et al (1975) which provides a theoretical study of the induced magnetic fields in the vicinity of a vertical land-sea interface. This study points out that the horizontal and vertical components of the magnetic field do not attenuate at similar rates for points inland, but rather that the horizontal component attenuates more rapidly than the vertical component. The ratio between the horizontal component and the vertical component is found to depend upon the wavelength, the ocean depth, and the position relative to the coast.

1.3 Rationale for the Choice of an Analogue Model Approach

In order to investigate the magnetic fields over structures with any degree of confidence in the results, a controlled and repeatable set of conditions is required. Such conditions are not readily available in nature, but several laboratory and mathematical means may be used to isolate the effect of each parameter. Basically the methods that can be used are (i) analytical solution, (ii) numerical solution, and (iii) laboratory analogue

modelling. Most of the references listed earlier have dealt with the problem of induction by ocean waves using the technique of analytical solution. Although this method is the most elegant of the three techniques, the mathematics involved quickly becomes complicated even for the relatively simple case of an ocean with uniform and finite depth. The coupling of the electromagnetic induction problem and the complex fluid dynamics problem occurs through the Lorentz equation, and the mechanics of the fluid flow must be solved before the electromagnetic problem can be set up. At this time, the author knows of only one attempt (leibo et al, 1975) to extend the analytical technique to cases of geological interest involving horizontal asymmetry. Leibo et al (1975) investigated the magnetic field induced by ocean waves in the vicinity of a coastline with a vertical sea-land interface, and found it necessary to state the solutions in the form of multi-dimensional integral equations!

For the cases involving horizontal asymmetry, the fields can be calculated using the less elegant numerical approach. In the numerical method, the fluid mechanical

problem can be reduced to a three dimensional finite difference set of equations, whose elements represent the particle velocity at a given time, and whose boundary conditions are set up to represent the ocean floor, the ocean surface, the coast, and so on. The source of the waves can be taken as infinitely far away from the coast. After the fluid mechanical problem has been solved, the velocity matrix can be used in an iterative solution to Maxwell's equations. The chief problem with this technique (apart from programming considerations) is the large number of individual calculations that the set of equations require. As an order of magnitude estimate, this process would require about 10^9 double precision (ie complex) floating multiplications, for every solution attempted.

Ng and Dosso (1970) carried out a feasibility study of the analogue model approach. They developed the basic scaling conditions, and investigated several technical aspects of designing a laboratory analogue model.

The technique of analogue modelling was chosen by the author in view of the study by Ng and Dosso (1970), since it promised useful results for complex ocean-land

boundaries and underwater structures. For the model results to be signifigant, great care must be taken in setting up the modelling conditions in the laboratory. The conditions must be accurately controlled and stable, since the ratio of the induced field to the background field is of the order of 10^{-5}. The background field must therefore be held steady well within one part in 10^{7}. Also the problem must not become hydromagnetic, which (assuming a modelling fluid of mercury), necessitates a background field whose magnitude is less than one kilogauss (10^{-1} T). This restriction, which becomes clear as the scaling conditions are derived, places an upper limit on the induced field of about 1000 gammas (10^{-6} T) as a result of the ratio of the induced field to the background field, hence a sensitive probe is required. To physically fit the problem into a laboratory, a linear scaling factor of about 10^{4} must be employed, hence the probe, used to measure the magnetic field, must also be small physically. The techniques employed by the author to meet these various criteria, and the results subsequently obtained, form the basis for this thesis.

CHAPTER 2

MATHEMATICAL ANALYSIS

2.1 Mathematical Expressions for a Uniform Depth Ocean

2.1.1 Infinite Depth Ocean

In the simplest geophysical problem concerning ocean wave induction of magnetic fields, the ocean is of infinite depth and has uniform conductivity σ. Fluid waves of small amplitude a_o propagate along the upper surface of this ocean in the x direction with phase velocity $\overline{V}$. The velocity of the fluid elements $\overline{v}$ is then given by (Coulson 1955)

$$\overline{v} = -a_o \omega \left(\hat{z} + i\hat{x} \right) \exp\left(i\omega t + \frac{i\omega^2}{g} z - \frac{i\omega^2}{g} x \right) , \quad (1)$$

where $\hat{z}$ and $\hat{x}$ are real unit vectors in the direction of the vertical and in the direction of the wave propagation respectively, ω is the radian frequency of the wave, $i=(-1)^{\frac{1}{2}}$, g is the acceleration due to gravity, and $z<0$ locates the ocean. After the appropriate boundary conditions have been satisfied, Maxwell's equations can be used to solve exactly for the electric and magnetic fields both in and above the ocean. Weaver (1965), quotes an approximate solution for the horizontal field B_x at a height h above the ocean,

$$B_x = -\tfrac{1}{2} i \mu \sigma a_o \hat{u}^* \cdot \hat{x} \left(\frac{g}{k} \right)^{\frac{1}{2}} \overline{F} \cdot \hat{u} \exp\left(-kh \right) , \quad (2)$$

where k is the wave number of the ocean wave, $\overline{F}$ is the background field, and $\hat{u}$ is a unit vector in the direction of particle velocity, and is given by

$$\hat{u} = 2^{-\frac{1}{2}} (\hat{Z} + i\hat{X}) \quad . \tag{3}$$

Here $\hat{Z}$ and $\hat{X}$ are now complex unit vectors in the direction of the vertical and in the direction of the wave propagation respectively, and each vary as exp $(-i\omega t)$, $\hat{u}^*$ is the complex conjugate of $\hat{u}$.

From (2), it can readily be seen that the magnitude of the induced field varies directly as the amplitude of the inducing field, and inversely with the period. This latter effect, combined with the exp(-kh) attenuation of the observed field, implies that the high frequency contribution to the induced field will be small at reasonable elevations over the ocean, and also that the main component of the induced signal will come from low freqnency swell. (These effects have been noted by many observers, including Semenov and Fonarev (1975)).

2.1.2 Finite Depth Ocean

For an ocean of finite depth d, it is necessary to invoke an expression derived by Podney (1975)

$$\overline{B} = \tfrac{1}{2} i\mu\sigma a_o \hat{u}^* \left[\frac{g}{k} \tanh(kd)\right]^{\frac{1}{2}} \left[\overline{F}\cdot\hat{u} + \left(\frac{kd}{\exp(2kd)-1}\right)\overline{F}\cdot\hat{u}^*\right] \exp(-kh) \tag{4}$$

This expression is still only valid if the waves are small in amplitude, and it presupposes a uniform, horizontal, and non-conductive ocean floor.

If the ocean bottom slopes, then the wave amplitude will increase as the coast is approached. This increase in wave height will naturally tend to increase the induced signal, which should consequently become enhanced. An approximate expression for this increase can be derived if it is assumed that the ocean is shallow ($d << \frac{\lambda}{2\pi}$).

In a simple harmonic oscillator undergoing small oscillations, the energy is equally divided between kinetic and potential forms, when considered as a time average (Goldstein, 1950). Per unit width of a surface wave, the average potential energy <E> per cycle is

$$\langle E \rangle = \int_0^{\lambda} \rho \, g \, \frac{[a(y)]^2}{2} \, dy \quad . \tag{5}$$

Since the height a(y) is harmonic, assume that it has the form

$$a(y) = a_o \sin \left(\frac{2\pi y}{\lambda} \right) \quad . \tag{6}$$

If this expression is substituted into Eq (5), and the resulting integral is evaluated, an expression for the average potential energy <E> is obtained,

$$\langle E \rangle = \frac{\pi \rho \, g \, a_o^2}{2} \quad , \tag{7}$$

which can be rewritten as

$$a_o^2 = \frac{2\langle E \rangle}{\pi \rho g \lambda} \quad . \tag{8}$$

If the energy of the wave is conserved, then <E> will be a constant as the wave advances up the slope, and Eq (8) will reduce to

$$a_o = \frac{c}{(\lambda)^{\frac{1}{2}}} \quad , \tag{9}$$

where λ is the wavelength of the wave, a_o is the amplitude of the wave, and c is a constant.

The velocity of a wave is given by $V=\lambda f$, and in the case of a shallow surface wave, by $V=(gd)^{\frac{1}{2}}$, leading to the expression,

$$\lambda = \frac{1}{f} (gd)^{\frac{1}{2}} \quad . \tag{10}$$

Since the frequency f of the wave is a constant, substituting (10) into (9) leads to the result

$$a_o(y) = \frac{c_1}{[\ d(y)\ ]^{\frac{1}{4}}} \quad , \tag{11}$$

where c_1 is another constant. This result states that the wave amplitude will vary as the inverse fourth root of the fluid depth. In general, a surface wave in a deep ocean will behave as though it had an effective depth d of one radian ($d = \frac{\lambda}{2\pi}$). Equation (11) then suggests that a wave produced in the deep ocean with wavelength λ near its source, will find its amplitude enhanced at depth d ($d << \frac{\lambda}{2\pi}$), given by

$$\frac{a_o}{a_\infty} = \left[\ \frac{\lambda}{2\ \pi\ d}\ \right]^{\frac{1}{4}} \quad , \tag{12}$$

as it moves up the slope toward the coast. The increase in wave height will tend to enhance the induced field, and as stated earlier, the signal should be expected to increase. Clearly, this enhancement cannot continue indefinitely as the fluid becomes increasingly shallow, and the limit to this enhancement appears in (4) as the factor $[\ \frac{\omega}{k}\ \tanh(kd)\ ]^{\frac{1}{2}}$, which reduces to $(gd)^{\frac{1}{2}}$ in the case of a shallow ocean. This factor clearly goes to zero as the depth decreases to zero, and in shallow water, the behaviour of Eq (4) can be characterized as the product of this term with the term $(\ \frac{1}{d}\ )^{\frac{1}{4}}$ (which enters through Eq (9)). In this case, the induced magnetic field $\overline{B}$ should approach zero as a function of the fourth root of the ocean depth.

2.2 Derivation of the Analogue Model Scaling Conditions

The laboratory analogue model is used to simulate an ocean of finite depth in the earth's magnetic field. This field is assumed to be vertical (ie, the inclination is taken to be 90^{o}) and uniform, the ocean is assumed to have an infinite horizontal extent, and the floor of the ocean is assumed to be non-conducting.

Mathematically, the scaled problem has a uniform magnetic field $\overline{F}$ which penetrates a fluid of conductivity σ and density ρ. Fluid surface waves propagate horizontally with phase velocity $\overline{V}$, while the fluid elements themselves have velocity $\bar{v}$. The motion of the fluid elements across the background field $\overline{F}$ induces a current of density $\overline{J}$.

To develop the scaling conditions, consider Maxwell's equations,

$$\nabla \cdot \overline{B} = 0 \quad , \tag{13}$$

$$\nabla \times \overline{E} = - \frac{d\overline{B}}{dt} \quad , \tag{14}$$

$$\nabla \cdot \overline{E} = \frac{\rho_e}{\varepsilon} \quad , \tag{15}$$

$$\nabla \times \overline{B} = \mu(\overline{J} + \varepsilon \frac{d\overline{E}}{dt}) \quad , \tag{16}$$

where $\overline{B}$ is the magnetic field induced by $\overline{J}$, and the Lorentz equation

$$\overline{J} = \sigma [\overline{E} + \bar{v} \times (\overline{B} + \overline{F})] \quad . \tag{17}$$

Substituting Eq (17) into Eq (16) yields

$$\nabla \times \bar{B} = \mu\sigma[\ \bar{E} + \bar{v} \times (\ \bar{B} + \bar{F}\ )] + \mu\varepsilon\frac{d\bar{E}}{dt} \quad .$$

Since the dimensions scaled are much smaller than the electromagnetic wavelengths, displacement currents can be ignored, and the expression reduces to

$$\nabla \times \bar{B} = \mu\sigma[\ \bar{E} + \bar{v} \times (\ \bar{B} + \bar{F}\ )] \quad .$$

Multiplying both sides of this equation by $\nabla\times$ to obtain

$$\nabla\times\nabla\times\bar{B} = \mu\sigma[\ \nabla\times\bar{E} + \nabla\times(\nabla\times(\bar{B} + \bar{F}))] \ ,$$

and using the identity

$$\nabla \times \nabla \times = \nabla(\ \nabla\cdot\ ) - \nabla^2 \quad ,$$

as well as Eqs (13) and (14),

$$\nabla^2\bar{B} = \mu\sigma[\ \frac{d\bar{B}}{dt} - \nabla\times(\ \bar{v} \times \bar{B}\ ) - \nabla\times(\ \bar{v} \times \bar{F}\ )] \qquad (18)$$

is obtained.

Assuming that the solution to (18) varies harmonically in time and space, the operators ∇ and $\frac{d}{dt}$ can then be replaced with $in\bar{k}$ and $-in\omega$ respectively, where n is the number of field variables multiplied together in the operand.

Equation (18) reduces to

$$k^2\bar{B} = i\mu[\ \sigma\omega\bar{B} + 2\sigma\bar{k} \times (\bar{v} \times \bar{B}) + \sigma\bar{k} \times (\bar{v} \times \bar{F})] \qquad (19)$$

Let geophysical parameters be represented by the primed symbols, then (19) for the geophysical problem becomes,

$$k'^2\bar{B}' = i\mu[\sigma'\omega'\bar{B}' + 2\sigma'\bar{k}'x(\bar{v}'x\bar{B}') + \sigma'\bar{k}'x(\bar{v}'x\bar{F}')] \qquad (20)$$

The variables in the model problem and the geophysical problem can be related by the linear transformations

$$k = k_o k' \ , \qquad \omega = \omega_o \omega' \ , \qquad B = B_o B' \ ,$$

$$v = v_o v' \ , \qquad \sigma = \sigma_o \sigma' \ , \qquad F = F_o F' \ ,$$

where k_o, ω_o, B_o, v_o, σ_o, and F_o are dimensionless quantities which shall be termed scale factors. Using these transformations, and assuming that the permeability remains constant ($\mu = \mu'$), Eq (20) becomes

$$k^2\bar{B} = i\mu[\alpha_1\sigma\omega\bar{B} + 2\alpha_2\sigma\bar{k}x(\bar{v}x\bar{B}) + \alpha_3\sigma\bar{k}x(\bar{v}x\bar{F})] \ , \qquad (21)$$

where $\alpha_1 = \dfrac{k_o^2}{\sigma_o\omega_o}$ $\qquad \alpha_2 = \dfrac{k_o}{\sigma_o v_o}$,

and $\alpha_3 = \dfrac{B_o k_o}{\sigma_o v_o F_o}$.

In order for the geophysical and the model problems to be equivalent, Eqs (20) and (21) must be equivalent. This will be the case if the dimensionless quantities α_1, α_2, and α_3 are of unit magnitude, leading to

$$\frac{\sigma\omega}{k^2} = \frac{\sigma'\omega'}{k'^2} \ , \qquad (22)$$

$$\frac{\sigma v}{k} = \frac{\sigma' v'}{k'} \ , \qquad (23)$$

$$\frac{\sigma v F}{B k} = \frac{\sigma' v' F'}{B' k'} \quad . \tag{24}$$

Dividing Eq (23) by Eq (24) leads to

$$\frac{B}{F} = \frac{B'}{F'} \quad ,$$

which implies that the ratio of the induced field to the primary field is fixed.

Consider now the fluid mechanical aspect of scaling. To demonstrate that the geophysical problem of ocean waves moving in the earth's magnetic field is a fluid mechanics problem rather than a magneto-hydrodynamics problem, it is necessary to show that the electromagnetic body forces are much less than the gravitational body forces. The electromagnetic body force is given by $\bar{J} \times \bar{F}$, and the current density $\bar{J}$ is approximately equal to $\sigma(\bar{v} \times \bar{F})$ from (17), hence the electromagnetic body force is approximately $\sigma(\bar{v} \times \bar{F}) \times \bar{F}$, which is of the order of $\sigma v F^2$. The gravitational body force is then given by ρg, hence the ratio of the gravitational body force to the electromagnetic body force is of the order of

$$R = \left(\frac{\rho g}{\sigma v F^2}\right) \quad . \tag{25}$$

Using ρ=1000 kg m^{-1}, g=10 m s^{-2}, σ=10 S m^{-1}, and F=10^{-2} T for the geophysical problem, leads to the ratio $R \sim 10^8$, which confirms the intuitive expectation that the magnetic field exerts a negligible body force on the ocean. Thus a large value of R will be required in the analogue model

to simulate the geophysical problem correctly.

The magnetic field also gives rise to an apparent viscosity in the conducting fluid. The signifigance of this induced viscosity is proportional to the dimensionless quantity M, termed the Hartmann number. This number is given by Ferraro and Plumpton (1961) as

$$M^2 = \frac{\sigma F^2 L^2}{\eta} \quad . \tag{26}$$

For sea water, M is large due to the large characteristic lengths involved. Hence the major factor contributing to viscosity will be the magnetic field (which will automatically scale), so that fluid effects can be ignored. A large value for M will also be required in the analogue model.

Given that electromagnetic coupling is small, and neglecting viscosity effects, Coulson (1955) calculates the phase velocity for a surface fluid wave to be

$$V' = \left[\left(\frac{g}{k} + \frac{k'\gamma'}{\rho'} \right) \tanh(kd) \right]^{\frac{1}{2}} \quad . \tag{27}$$

Here V' is the phase velocity, $k' = \frac{2\pi}{\lambda}$, the wave number, γ' the surface tension, ρ' the density, and d' the depth of the ocean.

Using this expression, and a similar expression for the model fluid, we can express the ratio of the wave velocity V in the model to the wave velocity V' in the ocean as

$$\left(\frac{V'}{V}\right) = \frac{\left(\frac{g}{k} + \frac{k\gamma}{\rho}\right)\tanh(kd)}{\left(\frac{g}{k'} + \frac{k'\gamma'}{\rho'}\right)\tanh(k'd')} \quad . \tag{28}$$

Since all lengths are scaled in the same manner, $\frac{d}{d'}=\frac{\lambda}{\lambda'}$, and since $k=\frac{2\pi}{\lambda}$, then $kd=k'd'$. It follows that $\tanh(kd)=\tanh(k'd')$, and (28) becomes

$$\left(\frac{V'}{V}\right)^2 = \frac{\left(\frac{g}{k} + \frac{k\gamma}{\rho}\right)}{\left(\frac{g}{k'} + \frac{k'\gamma'}{\rho'}\right)} \quad . \tag{29}$$

Using the expression for the phase velocity

$$V = \frac{\omega}{k} \quad , \qquad V' = \frac{\omega'}{k'} \quad ,$$

Eq (29) can be expressed as

$$\left(\frac{k'}{k}\right)^2 = \left(\frac{\omega'}{\omega}\right)^2 \frac{\left(\frac{g}{k} + \frac{k\gamma}{\rho}\right)}{\left(\frac{g}{k'} + \frac{k'\gamma'}{\rho'}\right)} \quad . \tag{30}$$

For ocean waves of wavelength $\lambda \sim 10^2$ m and surface tension $\gamma' \sim 10^{-1}$ N m^{-1}, the ratio $\frac{g}{k'} \sim 10^2$ m^2 s^{-2} is very much greater than the ratio $\frac{k'\gamma'}{\rho'} \sim 10^{-5}$ m^2 s^{-2}. Thus

$$\frac{g}{k} + \frac{k'\gamma'}{\rho'} \simeq \frac{g}{k} \quad . \tag{31}$$

If Eq (31) is substituted into (30), the resulting expression can be simplified to

$$\left(\frac{k'}{k}\right) = \left(\frac{\omega'}{\omega}\right)^2 \left(1 + \frac{k^2\gamma}{g\rho}\right) \quad . \tag{32}$$

If Eq (22) is used to substitute for $\frac{\omega'}{\omega}$ in (32), and recalling that kd=k'd', Eq (32) becomes

$$\frac{k'}{k} = \frac{d'}{d} = \left(\frac{\sigma}{\sigma'} \right)^{\frac{2}{3}} \left(1 + \frac{k^2 \gamma}{g \rho} \right)^{\frac{1}{3}} , \qquad (33)$$

which is the linear scaling factor. From (22) and again using kd=k'd', the frequency scaling obtained is

$$\frac{\omega'}{\omega} = \left(\frac{\sigma}{\sigma'} \right) \left(\frac{k'}{k} \right)^2 = \left(\frac{\sigma}{\sigma'} \right) \left(\frac{d}{d'} \right)^2 . \qquad (34)$$

Equations (33) and (34) contain the desired scaling factors, however (33) requires a knowledge of the wave number, which is rather difficult to measure experimentally. It is therefore desirable to express the scale factors in terms of frequency. This can be done by substituting the expression $\omega=Vk$ into (27), which leads to

$$\omega = k\left[\left(\frac{g}{k} + \frac{k\gamma}{\rho} \right) \tanh(kd) \right] . \qquad (35)$$

This equation must then be solved for the wave number k in terms of the frequency ω. The value for k thus obtained can be substituted into (33) to obtain the linear scaling factor and likewise substituted into (34) to obtain the frequency scaling factor. Thus it is possible to scale down both the electromagnetic and the mechanical aspects of the problem, and the task at hand is to suitably scale the geophysical dimensions to reasonable laboratory dimensions.

CHAPTER 3

THE LABORATORY ANALOGUE MODEL

3.1 Mercury as the Modelling Fluid

The analogue model employed a modelling fluid of mercury, which filled a small plywood box to a depth of 2.8 cm. This mercury 'ocean' was situated in a uniform vertical magnetic field with magnitude of approximagely 60 nanotesla. For ocean waves in the earth's magnetic field, the electromagnetic body force is negligible compared with the gravitational body force, as was shown through Eq (25) in chapter 2. This expression gives the ratio of gravitational to electromagnetic body force as

$$R \sim \frac{\rho g}{\sigma v F^2} \quad . \tag{25}$$

Using mercury as the model fluid, with $\rho \sim 10^4$ kg m^{-3}, $\sigma \sim 10^6$ S m^{-1}, $v \sim 10^{-1}$ m s^{71}, and a model magnetic field $F \sim 10^{-2}$ T, the resulting value for $R \sim 10^4$. Hence the electromagnetic body force can be ignored. The effect of fluid viscosity can be ignored if the Hartmann number M is small. This number is given by

$$M^2 = \frac{\sigma F^2 L^2}{\eta} \quad , \tag{26}$$

and for the model, using $\sigma \sim 10^6$ S m^{-1}, $F \sim 10^{-2}$ T, $L \sim 2 \times 10^{-2}$ m, and $\eta \sim 1.5$ kg m^{-1} s^{-1}, a value $M \sim .026$ is obtained. Thus the fluid viscosity can be ignored, in comparison with the magnetic viscosity.

3.2 The Analogue Model Construction and Measurement Technique

The model itself had two major components, namely a soft iron 'magnet box', used to produce the magnetic field, and a wooden box containing the mercury.

The magnet box (shown in Fig. 1) consisted of two horizontal soft iron plates (51 cm square x 6.6 cm thick), spaced 35 cm apart by two side plates. Three permanent magnets, with 6 cm pole gaps and approximately 10^{-1} T field strength, were clamped across each of the 6 cm gaps in the sides of the box as shown in Fig. 1. Over an ellipsoidal volume 15 cm x 20 cm x 20 cm in the central region of the magnet box, the field was approximately vertical and uniform to within better than 10%. Centered in this volume was a wooden box of dimensions 25 cm x 37 cm x 10 cm deep, filled to a depth d of mercury. This mercury box, supported by a sturdy wooden stand, was mechanically decoupled from the magnet box.

Various methods of generating waves in the mercury were examined. A very simple procedure, that of dropping an object into the mercury from a small fixed height, was perfected. After trying various shaped bodies, including spheres, hemispheres, half cylinders, and cylinders in the fluid, it was found that a horizontal lucite cylinder (12 cm long by 1.3 cm diameter) dropped from a height of 1 cm, produced a repeatable, monochromatic wave packet with appropriate amplitude. It was adopted as the standard wave generator for this experiment.

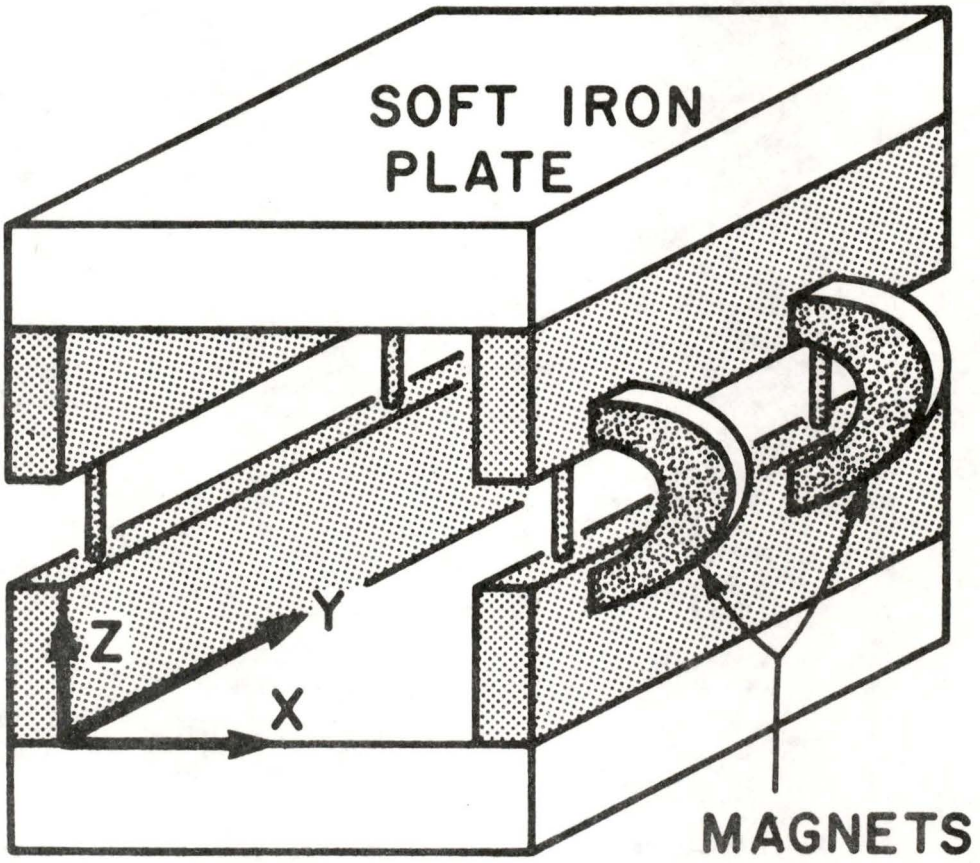

Fig. 1. The magnet box

Waves, approximately plane, propagated in the Y-direction perpendicular to the horizontal axis of the cylinder wave generator. The wave amplitude was measured with the aid of a long-threaded brass screw, which could be raised or lowered by turning to make or break electrical contact with the mercury surface. By adjusting the screw in very small increments, and repeatedly dropping the horizontal cylinder from a standard height, the wave amplitude was established. With care, repeatable measurements could readily be made.

A Hewlett-Packard model 428B fluxgate gaussmeter was used as a detector to measure the Y-component of the induced field. The waves in the fluid propagated in the Y-direction, and the position of the wave generator was selected to ensure that the interference from waves reflected from the tank walls was minimized. Since the primary field was (approximately) vertical, the residual Y-component (5×10^{-5} T) was easily cancelled out with the aid of a suitably positioned small permanent magnet (.8 cm long by .2 cm diameter), mounted on the sensing element of the gaussmeter probe. With the residual Y-component of the field in the detector element nulled, the gain setting of the gaussmeter could be increased to the point where signals less than 10^{-9} T could readily be detected. For a passing mercury wave, the resulting induced Y-component magnetic field detected by the gauss-

meter sensing element was amplified by a Princeton Applied Research model 225 preamplifier (set for a 1-10 Hz pass-band), and filtered by a PAR 217 high-pass (1 Hz) and a PAR 216 low-pass (10 Hz) filter system. A Tektronix 549 storage oscilloscope and camera were used to record the amplified signals. The noise level of the above apparatus, caused by vibrations of the magnet box, transients in cables, etc., was less than 10^{-9} T during measurements. A block diagram of the equipment used, and a typical photograph of an oscilloscope trace are shown in Fig. 2.

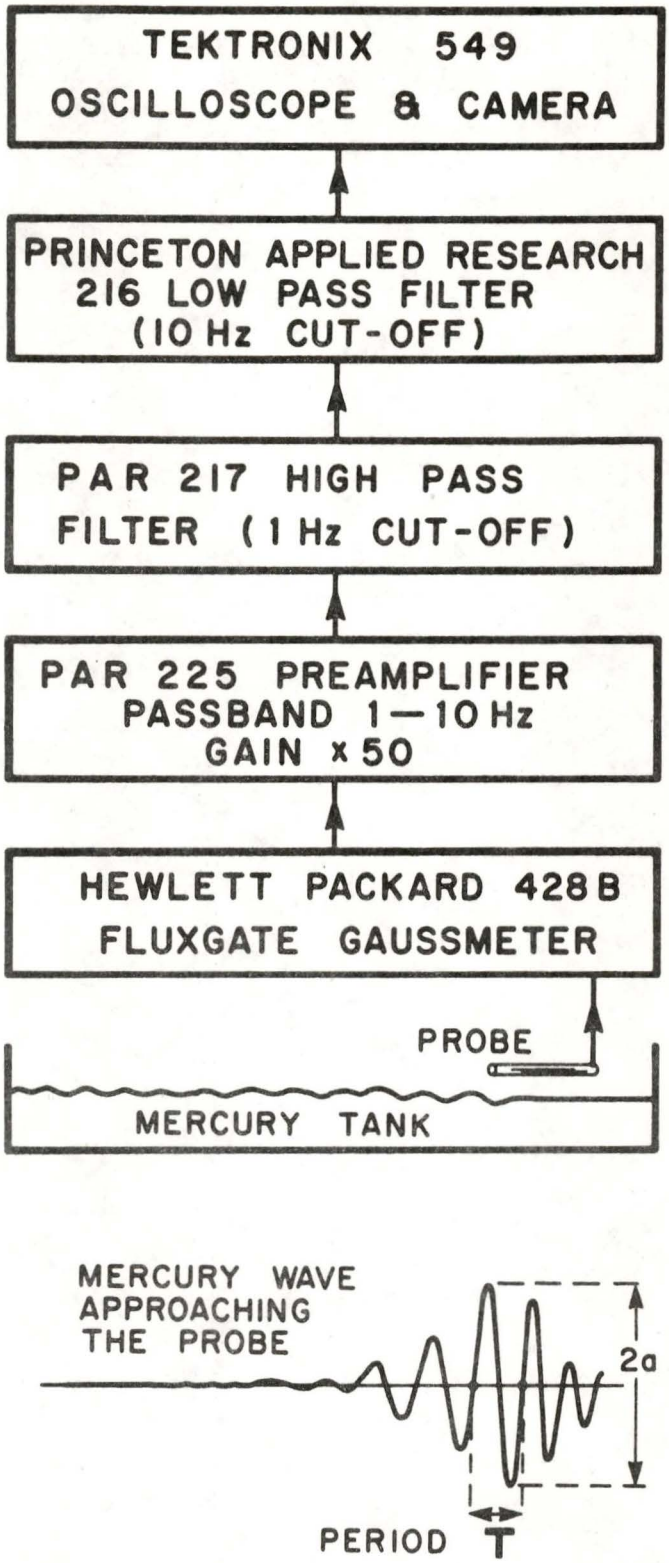

Fig. 2. Block diagram of the equipment and a typical oscilloscope wave trace.

3.3 Determination of the Validity of the Analogue Model Technique

With the aid of the wave-height detector described earlier, the wave height was measured for a series of three independent trials, and the results averaged. When the lucite cylinder wave generator was dropped from an elevation of 1.0 cm, the average wave height was 8.3×10^{-4} m with a variance of 2%. Using an RFL 3265 Hall-effect gaussmeter, the magnitude of the primary field F at the surface of the mercury was measured to be 6.6×10^{-3} T.

Photographs of the oscilloscope traces, for a series of three independent trials of measurements of the Y component B_y of the induced field, were used to determine the period and frequency of the mercury waves, as well as the amplitude of the induced magnetic field. The amplitude of the induced field was calculated from measurements of the amplitude of the photographed signal. The particular oscillation of the wave packet used is indicated in Fig. 2. The same oscillation was used to calculate the period and the frequency of the mercury waves.

The induced field measurements were averaged for three independent observations, giving an induced field amplitude for $B_y = 2.51 \times 10^{-7}$ T with a 2% variance, for a period of .211 seconds and a frequency of 4.73 Hz. Using the magnitudes of the primary field (6.6×10^{-3} T) and of the induced field (2.51×10^{-7} T), the ratio for $B_y/F = 3.8 \times 10^{-5}$ was obtained.

Using the frequency of 4.73 Hz, as well as the other appropriate model parameters in Eq (35), the model wavelength was determined to be λ=6.84 cm. This wavelength was used in Eq (35) to obtain the linear scale factor $d'/d=3.81 \times 10^{-3}$, and the linear scale factor was used in Eq (34) to determine the frequency scale factor $f'/f=1.60 \times 10^{-2}$. With the scale factors established, the geophysical parameters simulated by the analogue model were determined. To examine the validity of the model, the theoretical value of the ratio B'/F' was calculated using Podney's (1975) expression (Eq (4)) for the model parameters. Then, using the condition B/F=B'/F', the analogue model field ratio could be compared directly with the field ratios calculated using Podney's (1975) expression for a finite uniform depth fluid. For interest, the ratio B_y'/F' was also calculated for the case of an ocean of infinite depth, using Weaver's (1965) expression (Eq (2)).

Analogue model parameters, the geophysical parameters, the scale factors, and the values of the measured and theoretically calculated field ratios are shown in Table I. From this table, it is evident that the experimental field ratio ($B_y/F=3.80 \times 10^{-5}$) agrees very well with the calculated field ratio ($B_y/F=3.78 \times 10^{-5}$) for the model parameters used. The estimated experimental error for the model results lies between 5% and 10%.

TABLE I

Summary of analogue model parameters, geophysical parameters, and measured and computed values.

	Model	Geophysical
Fluid depth	$d = 2.0$ cm	$d' = 76$ m
Fluid conductivity	$\sigma = 1.04 \times 10^{6}$ S m^{-1}	$\sigma' = 4.50$ Sm-1
Probe height	$h = 1.0$ cm	$h' = 38$ m
Wave amplitude	$a_o = .082$ cm	$a_o' = 3.1$ m
Wavelength	$\lambda = 6.84$ cm	$\lambda' = 261$ m
Period	$T = .211$ s	$T' = 13.2$ s
Frequency	$f = 4.73$ Hz	$f' = .0757$ Hz
Angular frequency	$\omega = 29.8\ s^{-1}$	$\omega' = .476\ s^{-1}$
Surface tension	$\gamma = .487$ N m^{-1}	
Primary field	$F = 6.6 \times 10^{-3}$ T	$(6.6 \times 10^{1}$ Gauss)
Induced field	$B_y = 2.51 \times 10^{-7}$ T	$(2.51 \times 10^{-3}$ Gauss)

Scale Factors

Conductivity scale factor	$\sigma'/\sigma = 3.33 \times 10^{-6}$
Linear scale factor	$d'/d = 3.81 \times 10^{3}$
Frequency scale factor	$f'/f = 1.60 \times 10^{-2}$

Field Ratios

Analogue Model for 2 cm mercury	$B_y/F = 3.80 \times 10^{-5}$
Podney (1975) for 76 m ocean	$B_y'/F' = 3.78 \times 10^{-5}$
Weaver (1965) for ∞ depth ocean	$B_y'/F' = 3.54 \times 10^{-5}$

In summary, the excellent agreement between the theoretical and observed field ratios suggests that the analogue model technique is valid. Thus the analogue model technique should be valid for studying more complex cases, as for example, an ocean with an irregular bottom.

CHAPTER 4

DISCUSSION OF THE ANALOGUE MODEL MEASUREMENTS

4.1 Introduction

In chapter 3 the validity of the experimental analogue model technique was examined for the case of a shallow uniform depth model ocean by comparing model results with theoretical calculations. With the validity established for the case of a uniform depth ocean, the model will now be extended to study cases of non-uniform ocean depths and sea-land interfaces. Measurements for these cases will be compared with measurements for the uniform depth model, in other words, the uniform depth case will be used as a "reference". Departures from the reference results will be attributed to the effect of changing ocean depth for the particular model. The models to be studied are (i) uniform depth model, (ii) step and shelf model, (iii) wedge and shelf model, (iv) dyke model, (v) sea mount model, (vi) sloping bay and shelf model, and (vii) reef and shelf model. Since changes in ocean depth affect the linear scaling factor, it is necessary to demonstrate that the effect of any such changes on the scale factor can be ignored. This demonstration has been relegated to appendix A.

4.2 The Uniform Depth Ocean Model

To study an ocean of uniform depth, a mercury depth of 2.8 cm was used in a vertical magnetic field of 5.7×10^{-3} T, simulating an ocean of depth 106 meters in a vertical magnetic field of 5×10^{-5} T. To establish a reference curve for comparison purposes, measurements were made in the manner described in chapter three, with the difference that rather than carrying out measurements at one point over the model fluid, a series of measurements were made for many points for a traverse along the Y direction covering a distance of at least 20 cm. The magnetometer probe, mounted on a rail attached to the upper plate of the magnet box, could be accurately positioned (at a height of 0.6 cm above the mercury) for points along the traverse. The wave generator was positioned 5 cm (Y=-8 cm in the diagrams) from one end of the tank, and the height of drop of the lucite cylinder generating the waves was 0.5 cm for all measurements. The procedure used in carrying out a measurement at a point was to position the probe at the desired location, generate a mercury wave, and photograph the resulting oscilloscope trace. The probe was then moved to the next point, and the procedure repeated. The linear scale factor and the frequency scale factor used here are somewhat different from those used in checking

the validity of the model in the earlier part of this work, since the model frequency now used is slightly different. In order to minimize difficulties associated with reflections for points near the tank wall (near Y=20 cm), the leading pulse in the fluid wave train was selected for all measurements, and this corresponded to a lower frequency than that used earlier. As before, the scale factors $d'/d = 3.77 \times 10^{3}$, $f'/f = 1.62 \times 10^{-2}$ were calculated using Eqs (33), (34) and (36). Using these scaling factors, 1 cm in the model corresponds to 38 m in the ocean, a wavelength of 9.5 cm in the mercury simulates a wavelength of 358 m in the ocean, and a frequency of 4 Hz in the model simulates a frequency of .064 Hz in the ocean. The probe height of 0.6 cm above the mercury corresponds to a height of 23 m above the surface of the ocean, and for the wavelength λ=9.5 cm, the mercury depth of 2.8 cm was of the order of 1/3 λ (1.9 radians).

Figure 3 shows the induced magnetic field as measured at points along the traverse over the surface of the model ocean of uniform depth d=2.8 cm. With the wave source located at Y=-8 cm, it is seen that the induced field initially falls off rapidly with distance from the source, and then becomes essentially uniform in the vicinity of Y=10 cm. Thus in the region Y=10 cm to Y=20 cm, the fluid waves are approximately plane. The mercury box

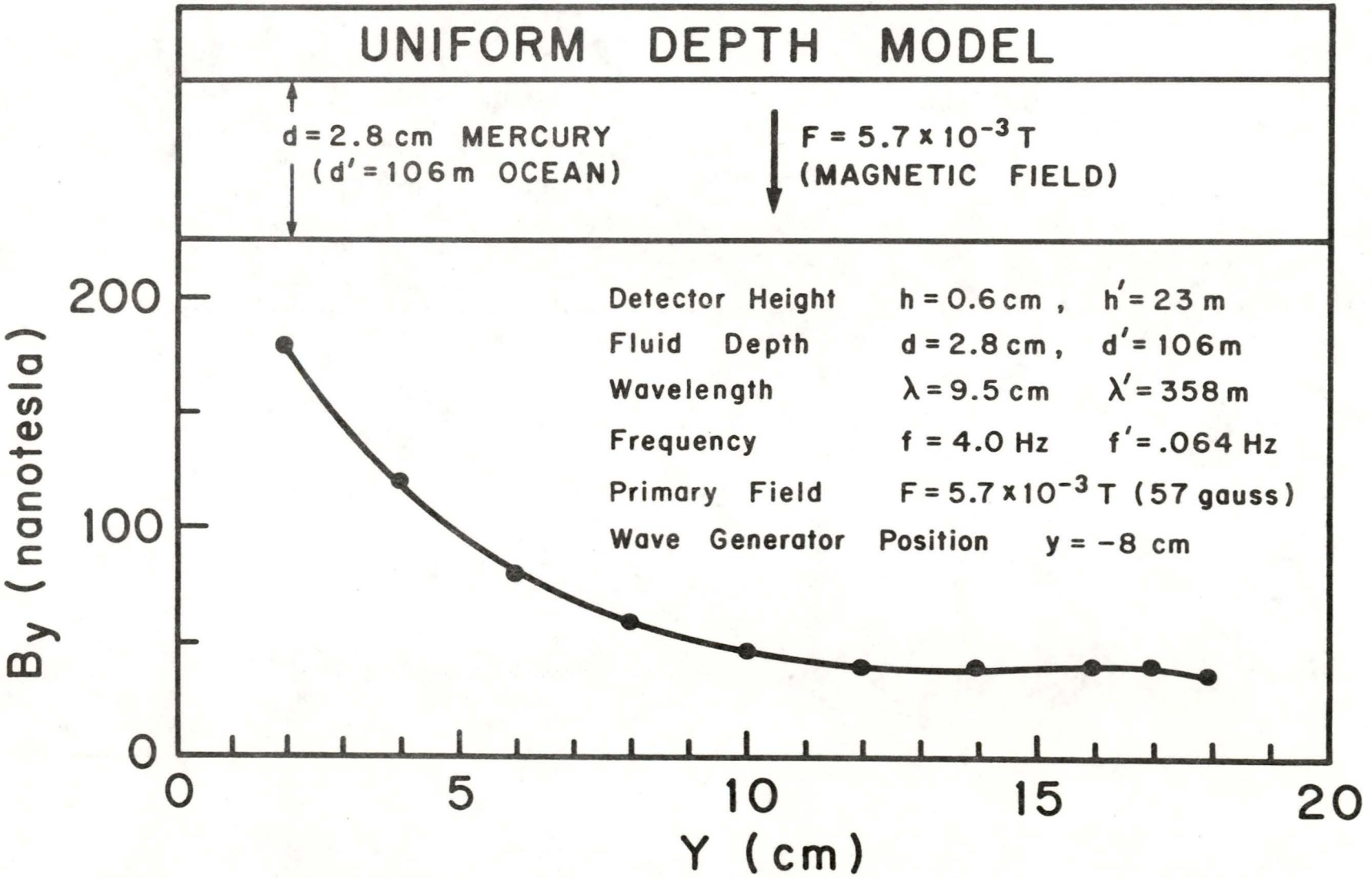

Fig. 3. Horizontal magnetic field induced by a fluid wave for a traverse over the uniform depth model.

was positioned in the magnet box so that this region was located in the region where the magnetic field was uniform. The curve in Fig. 3, for the uniform depth model, is used as a reference curve for comparison pusposes in studying the models shown in Figs. 4-6.

4.3 The Step and Shelf Model

To simulate a vertical discontinuity in a flat ocean floor, a non-conducting block was positioned at one end of the tank as shown in the upper part of Fig. 4a. A series of 5 blocks was used to permit studying the effect of changing shelf depth d_1. With the uniform depth region held at a constant depth d=2.8 cm, measurements were carried out for traverses over the mercury and embedded block. The curves in Fig. 4a show the magnetic field amplitude for five shelf depths d_1=0, .15, .4, .6, 1 cm (curves 1 - 5), simulating shelf depths of 0, 5.7, 15.2, 22.7, 38 meters in the geophysical case. The case of d_1=0 cm is the simple earth-sea vertical interface model sometimes used in simplified analytical induction studies. The other models (d_1>0) simulate a vertical earth-sea interface followed by a uniform depth shallow ocean near a coastline. It is to be noted that for curve 1, the

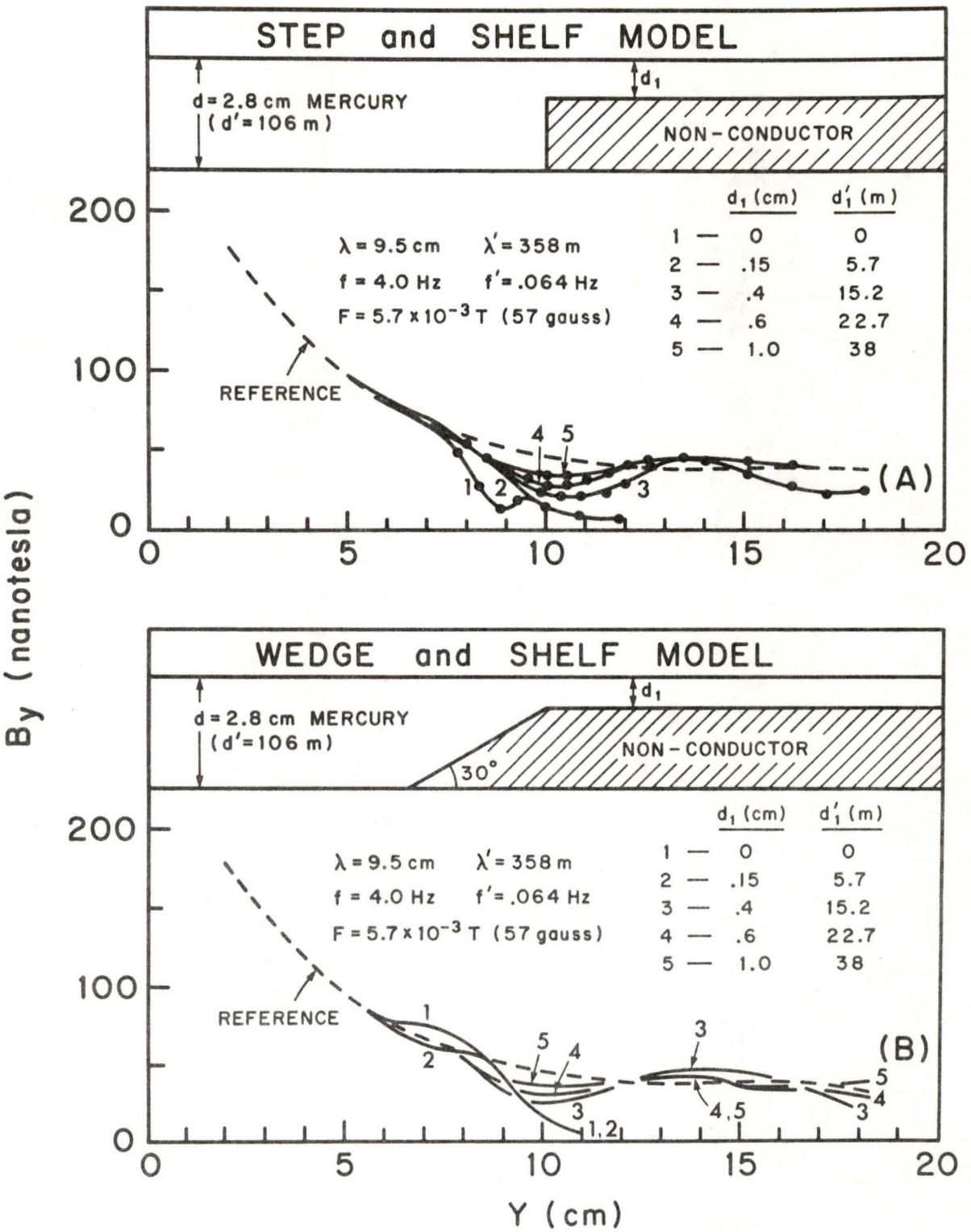

Fig. 4. Horizontal magnetic field induced by a fluid wave over the (a) step and shelf model and the (b) wedge and shelf model

amplitude of the induced field drops suddenly as the vertical interface is approached, rises somewhat near the interface, decaying over the shelf. The amplitude of the induced field, shown in curve 2, also decays as the step is approached, but the attenuation is more gradual, and in addition monotonic, compared with the attenuation noted for curve 1. For each of the other 3 curves, corresponding to shelf depths of .4, .6, 1 cm (15.2, 22.7, 38 m), the attenuation is not pronounced, and has a field minimum directly over the step. The field then builds up over the shelf, attaining a maximum value slightly greater than the reference field, at a distance of 4 cm (152 m) from the vertical interface. The minimum value over the shelf decreases as the ocean depth over the shelf increases. As the depth d_1 increases further, the fields should approach the reference values. The attenuation at the step, and the build-up of the field over the shelf can be explained in part as due to the modification of the waves as they pass from the deep ocean to the shallow ocean, and in part in terms of the changing induced electric current distribution caused by the abrupt change in ocean depth. The increasing wave amplitude for a range of decreasing fluid depths would tend to enhance the field, but this enhancement is insufficient to overcome the reduction in the efficiency of the induction process over the shallower

ocean, a net attenuation will result relative to the uniform depth ocean, as shown in appendix B. The observed enhancement must be due to the abrupt transition from the deep ocean to the shallow ocean, resulting in interference of the fluid waves, and abrupt shifts in the induced electric current pattern. The zone of maximum enhancement is situated approximately 4 cm behind the vertical interface, and signifigantly, 4 cm corresponds roughly to a distance of half a wavelength.

4.4 The Wedge and Shelf Model

To simulate the more realistic case of a sloping ocean floor and a shelf near a coastline, a non-conducting (lucite) block with a wedge-shaped (30°) leading edge was positioned as shown in the upper part of Fig. 4b. Again, with the uniform depth region held constant at d=2.8 cm, measurements were carried out for traverses over the embedded wedge and shelf model for the same shelf depths as used for the step and shelf model (Fig. 4a). For $d_1=0$, the model simulates the geophysical case of a shallow uniform depth ocean having a 30° sloping floor near the coastline. In curve 1, the amplitude of the induced field builds up over the ramp, becoming a maximum approximately half way up, and then falls off sharply as the coastline is approached further. This enhancement begins just beyond the point

where the uniform depth ocean floor contacts the sloping region. Somewhat similar behaviour is observed for the very shallow shelf depth of curve 2, with the field falling off sharply again as the shelf is approached. For each of the other 3 curves, corresponding to .4, .6, 1 cm(15.2, 22.7 38 m), there is essentially no enhancement over the ramp, but a minimum directly over the shelf edge is observed. As in the case of the step and shelf model, the field builds up over the shelf, attaining a value slightly greater than the reference field at a distance of 4 cm (152 m) from the leading edge of the shelf. The enhancement over the ramp, unique to the model wedge and shelf structure, could be caused by several factors. The gradual decrease in ocean depth will cause the wave amplitude to build up, in accordance with Eq (11) and the gentle transition between the deep ocean and the shallow shelf will tend to reduce interference effects in the wedge and shelf model, as compared to the step and shelf model. The currents will not change so abruptly near the interface, and the transition effects should be reduced. These factors should have less signifigance away from the transition region, and hence the behaviour of the field should be similar for both models, away from the transition. As expected, the observed field approached the reference field, as the shelf depth is increased.

4.5 The Dyke Model

To simulate a submerged dyke with vertical walls in a flat ocean floor, a non-conducting block, simulating a dyke, was positioned in the central region of the tank, as shown in Fig. 5a. A series of 4 blocks was used to investigate the effect of changing the depth of fluid d_1 over the dyke. The curves in Fig. 5a show the magnetic field amplitude for depths d_1=.2, .4, .6, 1 cm (curves 1-4), simulating fluid depths of 7.6, 15.2, 22.8, 38 m over a dyke in the geophysical case. As noted previously for the step and shelf model, a distinct minimum again occurs near the leading edge of the dyke (Y=5 cm). This minimum is followed by an enhancement of the field over the dyke, with the level of enhancement, and the depth of the minimum being greatest for shallow depths, with the exception of curve 1. In curve 1 for the case d_1=.2 cm (7.6 m), there is a small enhancement over the dyke following the minimum at the edge of the dyke, but the amplitudes for all points are well below the reference values (dashed line). These enhancements are probably due to interference effects at the vertical interfaces, and in this connection it is necessary to point out that they all occur approximately one half wavelength away from the preceding minima. Curve 1 shows the enhancement occurring only 2 cm from the preceding minimum, but at a depth of .2 cm, the wavelength is reduced to 3.5 cm as shown in appendix B.

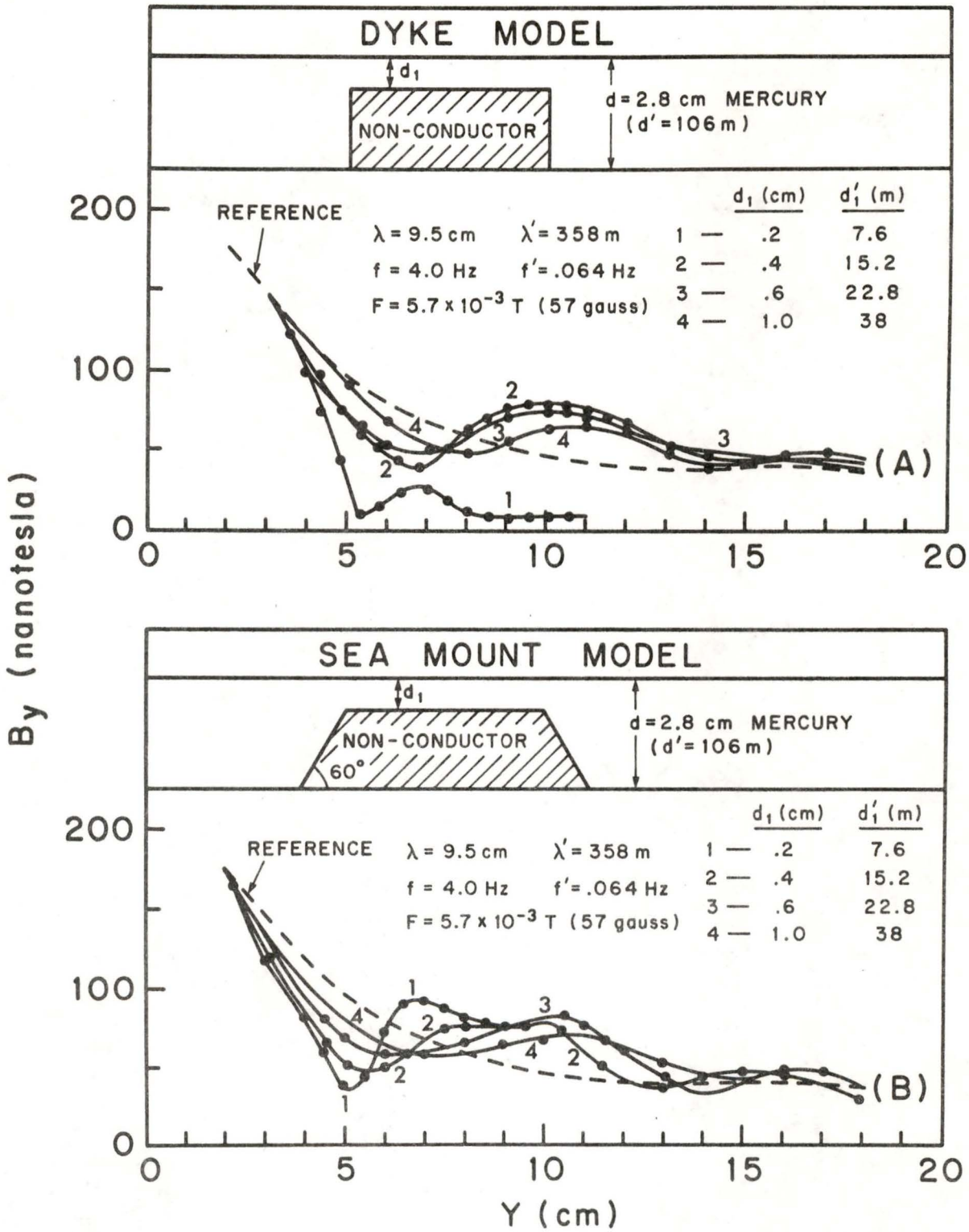

Fig. 5. Horizontal magnetic field induced by a fluid wave over the (a) dyke model and the (b) sea mount model

At positions well away from the dyke, the induced field observed approaches the reference field (except for curve 1). The return of the observed field beyond the dyke to the reference field value suggests that the effect of the dyke on the current system and the fluid wave is local to the region of the dyke, conversely the lack of such return for curve 1 suggests that signifigant attenuation occurs for fluid depths near .2 cm (corresponding to geophysical depths of 7.6 m).

4.6 The Sea Mount Model

To simulate the case of a submerged sea mount on a flat ocean floor, a two dimensional sea mount model, consisting of a non-conducting block with 60° sides, was positioned in the central region of the tank as shown in the upper part of Fig. 5b. To aid in the comparison, the sea mount model was positioned so that the upper portion of the model was in the same location as was the case for the dyke model of Fig. 5a. As noted for the dyke model, a distinct minimum occurs near the leading edge of the structure (Y=5 cm), and this minimum is observed for all depths of the sea mount. No enhancement, as distinct from that observed for the 30° wedge of Fig. 4b, is observed over the ramp, rather, the ramp serves to extend this minimum in the direction of the source. Enhancement is

noted over the horizontal portion of the mount, with the region of enhancement being well-defined. The curves for the shallowest depths (curves 1 and 2) display a double peak structure in the enhancement, whereas the curves for greater fluid depth (d_1=.6, 1 cm) display a broader and smoother maximum. Such a behaviour could be produced by shifts in the current distribution over the mount, and by interference effects between the leading and trailing edges of the mount. In all cases, the separation between the minimum and the region of enhancement was approximately one half of a wavelength, in the region over the mount. The minimum near the leading edge of the mount, and the subsequent enhancement became much less pronounced, as the depth of fluid over the mount was increased, with the induced field approaching the reference values. At positions well beyond the dyke (Y>15 cm) all curves approached the reference curve, suggesting that the waves did not experience much attenuation in their propagation over the mount. In contrast to the case for the dyke model (Fig. 4a), a block .2 cm below the surface had little effect on the induced field for Y>15 cm, suggesting that the attenuation of the field by the dyke for d_1=.2 cm was due to losses caused by the vertical nature of the interfaces.

4.7 The Sloping Bay and Shelf Model

To simulate a sloping ocean floor near a coastline for the case of a bay, a non-conducting block with an inverted conical (30°) frustrum with maximum radius d_2=5 cm, milled from the edge of the block was positioned in the tank, as shown in the upper part of Fig. 6a. Thus, the bay was semi-circular with the sloping region meeting the shelf at Y=10 cm along the traverse indicated in Fig. 6a. Measurements were taken for traverses through the center of the bay, the curves in Fig. 6a showing the magnetic field amplitude for five shelf depths d_1=0, .2, .4, .6, 1 cm (curves 1 - 5), simulating shelf depths of 0, 7.6, 15.2, 22.7, 38 m in the geophysical case. The case of d_1=0 cm is the simple sloping bay model at the edge of a coast, and the other models simulate depressions of various depths at the edge of a submerged shelf. It is to be noted that for curve 1, the induced field drops almost linearly, reaching a negligible value for Y=8 cm (2 cm from the bay-land boundary). There is, however, a noticeable drop in field intensity near Y=5 cm, for curve 1, and this drop coincides with the focal point of the bay. The other curves, corresponding to greater shelf depths, did not display any sudden changes near Y=5 cm, suggesting that signifigant reflection did not occur at the bay-land

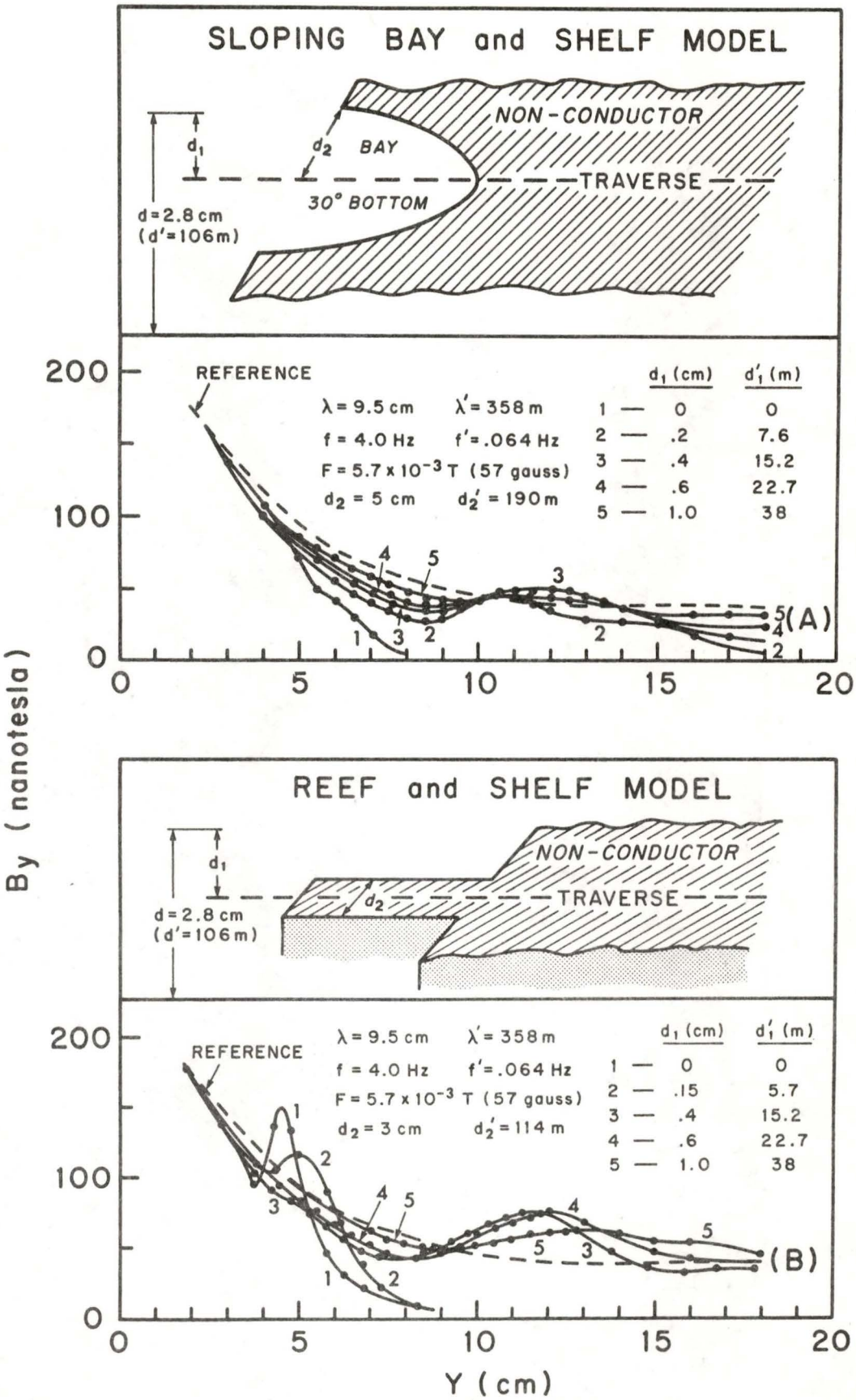

Fig. 6. Horizontal magnetic field induced by a fluid wave over the (a) sloping bay and shelf model and the (b) reef and shelf model

boundary for these depths. For curves 2,3,4,5 the field over the bay is attenuated relative to the reference field, the amount of attenuation being greatest for shallow fluid depths. This attenuation was characterized by a broad horizontal extent and was probably caused by channelling of electric currents from the shallow shelf to the bay, or to the departure from plane waves through the focussing effect of the geometry of the bay. The minima shifted to the right with increasing shelf depth, again in keeping with the change in wavelength with fluid depth. A signi-figant interference effect would be expected, since the bay has a radius of 5 cm, which is of the order of half a wavelength. Over the shelf, there is an enhancement of the fields, and this enhancement agrees qualitatively with the similar enhancement observed for the step and shelf model of Fig. 4a. As the depth of the shelf becomes large, the induced field along the traverse over the structure approaches the reference field value.

4.8 The Reef and Shelf Model

To simulate a reef perpendicular to a coastline, a non-conducting body of the form shown in Fig. 6b was positioned in the tank. The reef took the form of a 5 cm long rectangular prism projecting from the vertical side of a block. For ease of comparison with Fig. 6a, the

vertical side of the block, which also locates the shelf edge, was located at Y=10 cm. A series of 5 reef and shelf models was used to investigate the effect of changing shelf depth d_1. With the uniform depth region held at a constant depth d=2.8 cm, measurements were carried out for a traverse along the long dimension of the reef, as shown in Fig. 6b. The curves in Fig. 6b show the magnetic field amplitude for five shelf depths d_1=0, .15, .4, .6, 1 cm (curves 1 - 5) corresponding to shelf depths of 0, 5.7, 15.2, 22.7, 38 m in the geophysical case. The case of d_1=0 represents a narrow peninsula jutting out from a vertical sea-land coast. The other cases (d_1>0) represent submerged reefs extending from submerged shelves of uniform depth. It is to be noted that curves 1 and 2 display a marked enhancement at the tip of the reef (Y=5 cm), and then decay monotonically over the reef. The decay is consistent with the step and shelf model results of Fig. 4a, and the enhancement was a peculiarity of the reef structure, due probably to channelling of induced currents around the leading edge of the reef, and the changing nature of the wave front, departing from a plane wave front due to the interference with the reef. Current channelling would be expected since the reef obstructs the normal flow of electric current perpendicular to the

direction of wave propagation, producing a high current density in the fluid just beyond the tip of the reef. This high density of electric currents could to a large extent account for the magnetic field enhancement observed in the region beyond the tip, and the lack of an enhancement at the tip of the reef for greater depths indicates that there is sufficient fluid over these deep reefs so that the normal electric current flow is not impaired. These deep reefs also have little effect on the linearity of the wave front, so that focussing is essentially absent.

CHAPTER 5

CONCLUSIONS

The analogue model technique has been developed and used to investigate the magnetic field induced by ocean waves interacting with a variety of structures. The validity of this modelling technique for a uniform depth ocean has been established by comparison with calculations based on the theoretical predictions of Podney (1975), and the technique itself extended so as to investigate cases of non-uniform ocean depths and sea-land interfaces. In order to study these cases, measurements for these models have been compared with the (reference) measurements for the uniform depth model. As the depth of fluid over the non-uniformity in the various models approached the depth of fluid in the uniform depth model, the induced magnetic field approached the magnetic field observed for the reference.

To simulate a vertical discontinuity in a flat ocean floor, a step and shelf model with simulated shelf depths ranging from 0 to 38 meters was used. The major features of this model were a minimum in the magnetic field at the vertical interface, and an enhancement at a distance approximately one half wavelength beyond, over the shelf (Fig. 4a). The attenuation of the magnetic field at the interface, and the following enhancement became less pronounced as the depth of fluid over the shelf (d_1 in Fig. 4a) was reduced. The attenuation of the magnetic field at the vertical interface, and the enhancement of the field

over the shelf might be caused in part by the modification of the fluid waves as they pass from the deep ocean to the shallow ocean, and in part by the changing induced electric current distribution caused by the abrupt change in ocean depth. The increasing wave amplitude for a range of decreasing fluid depths would tend to enhance the field, but this enhancement should be insufficient to overcome the reduction in the efficiency of the induction process over the shallower ocean, and a net attenuation will result, as shown in appendix B. The observed enhancement must be due to the abrupt transition from the deep ocean to the shallow ocean resulting in interference of the wave motion, and abrupt shifts in the induced current pattern.

A wedge and shelf model, again with simulated shelf depths ranging fron 0 to 38 meters, was used (Fig. 4b) to simulate the more realistic case of a sloping ocean floor and shelf near a coastline. The behaviour of the induced field for this model was in most respects similar to the behaviour noted previously for the step and shelf model (Fig. 4a) as expected from the similar model geometries, with the major difference between the two results occurring in the region between Y=6 cm and Y=10 cm, ie, the simulated range of approximately 150 meters from the shelf edge. In this region, the wedge and shelf model had a 30° ramp, and over this ramp an enhancement of the magnetic field was noted for the very shallow shelf depths of 0 and 5.7 m (curves 1 and 2 in Fig. 4b). This enhancement unique to the model wedge and shelf structure, could be

caused by several factors. The gradual decrease in ocean depth would cause the wave amplitude to build up, in accordance with Eq (11) and the gentle transition between the deep ocean and the shallow shelf would tend to reduce interference effects. The electric currents will not change so abruptly near the interface, and so the effect of the transition between the deep ocean and the shallow shelf should be reduced. These factors have less signifigance away from the transition region, and hence the behaviour of the field is similar for both models (Fig. 4a and 4b) away from the interface region.

A model dyke, with simulated fluid depths ranging from 7.6 to 38 m, was employed (Fig. 5a) to simulate a submerged dyke with vertical walls. The results for this model also showed a minimum in the magnetic field near the vertical interface of the dyke (Y=5 cm) on the source side, with a subsequent enhancement at approximately half a wavelength beyond this minimum. The wavelength decreased with decreasing fluid depth as shown in appendix B, and this is in general agreement with the enhancement over the shelf shifting to the left as the shelf depth decreases. The level of enhancement is much greater than any level observed over the step and shelf model, or the similar wedge and shelf model, and a signifigant factor to consider is the 190 m (5 cm in the model) width of the dyke, which is of the order of half a wavelength for the approaching wave.

Thus various interference effects could be expected to occur between the leading and trailing vertical interfaces of the dyke. At positions well beyond the dyke, the induced field observed approaches the reference field (except for curve 1). The return of the observed field beyond the dyke to the reference field value suggests that the effect of the dyke on the current system and the fluid wave is local to the region of the dyke, conversely the lack of such return for curve 1 suggests that significant attenuation occurs for simulated ocean depths of the order of 15 m (curve 2).

A two dimensional sea mount model with simulated depths ranging from 7.6 to 38 m was used (Fig. 5b) to simulate the case of a submerged sea mount. The sea mount results were qualitatively similar to the results obtained for the dyke, in that there occurred a minimum at the edge of the sea mount facing the source (Y=5 cm in Fig. 5b), followed by a pronounced enhancement approximately half a wavelength beyond this minimum. No enhancement was observed over either ramp (60° sides) of the sea mount (as distinct to the enhancement observed for the 30° wedge of Fig. 4b), and the minimum near the leading edge of the shelf was broadened as the fluid depth increased. The enhancement noted over the horizontal portion of the mount was well-defined, displaying a double-peaked structure for the very shallow depths of 7.6 m and 15.2 m (curves 1 and 2 of Fig. 5b). Again, in keeping with the decrease in

wavelength with decreasing fluid depth, the enhancements of the magnetic field following the minima, shifted to the left as the fluid depth was decreased. For the deeper mounts of 22.8 and 38 m (curves 3 and 4 of Fig. 5b), as well as for positions greater than approximately 200 m (Y=15 cm in Fig. 5b) beyond the mount, the field approached the reference field, the latter suggesting that waves did not experience much attenuation in their propagation over the mount. In contrast to the case for the dyke model (Fig. 5a) for which a simulated depth of 15.2 m had little effect on the induced field for 200 m beyond (Y=15 cm in Fig. 5a) the interface, this suggested that the attenuation of the field by the dyke for a 7.6 m depth (curve 2 in Fig. 5a) was due to losses caused by the vertical nature of the interfaces.

A bay and shelf model, with simulated shelf depths ranging from 0 to 38 m, was used (Fig. 6a) to simulate a sloping ocean floor near a coastline for the case of a bay. The induced fields were observed to follow the general pattern of a minimum near the leading edge of the structure, followed by an enhancement over the shelf. Curve 1 (d_1=0) represents the simple sloping bay model at the edge of a coast, and for this case, the induced field decreases almost linearly, reaching a negligible value approximately 5 m from the bay-land boundary (curve 1) with the exception of a noticeable decrease in field

intensity approximately 190 m from the bay-land boundary (Y=5 cm in Fig. 6a), the location of which coincides with the focal point of the bay. The other curves, corresponding to greater shelf depths, did not display any sudden changes near this point, but the whole region of the bay was marked by a signifigant attenuation of the induced field as compared with the reference field, the amount of attenuation being greatest for shallow fluid depths. This attenuation was of broad horizontal extent and was due in part to channelling of electric currents from the shallow shelf to the bay, and in part was due to the departure from plane waves through the focussing effect of the geometry of the bay. The minima shifted to the right with increasing shelf depth, again in keeping with the change in wavelength with fluid depth. A signifigant interference effect would be expected, since the bay has a radius of 190 m, which is of the order of half a wavelength.

A reef and shelf model, simulating reef and shelf depths ranging from 0 to 38 m, was used (Fig. 6b) to simulate a reef perpendicular to a coastline, followed by a shelf. The induced field displayed a pronounced enhancement at the tip (Y=5 cm) of the very shallow reefs of 0 and 5.7 m (curves 1 and 2 in Fig. 6b), followed by an attenuation which was present over the length of the reef for all depths d_1. The decay was consistent with the step and shelf model results of Fig. 4a, and the enhancement was a peculiarity of the reef structure, due probably to

channelling of induced currents around the leading edge of the reef and the changing nature of the wave front, departing from a plane wave front due to the interference with the reef. Current channelling would be expected since the reef obstructs the normal flow of electric current perpendicular to the direction of wave propagation, producing a high current density in the fluid just beyond the tip of the reef. This high density of electric currents could to a large extent account for the magnetic field enhancement observed in the region beyond the tip, and the lack of an enhancement at the tip of the reef for greater depths indicates that there is sufficient fluid over these deep reefs so that the normal electric current flow is not signifigantly impaired. These deep reefs also have little effect on the linearity of the wave front, so that focussing is essentially absent.

Several interesting features of the horizontal induced magnetic field have been brought out by means of these analogue models. For shallow ocean depths over a submerged obstacle of large horizontal extent, the induced horizontal magnetic field is attenuated over the leading edge of the structure, with the attenuation being strongly dependent on the depth. Beyond the leading edge, the field is enhanced, reaching a maximum at a distance of approximately half a wavelength, and then decays toward a value consistent with the field expected over an ocean of the appropriate uniform depth. Further, the shape of the leading edge of

the structure can have an important effect on the fields for the very shallow fluid depths, this being brought out for the models having vertical, 60^{o} and 30^{o} interfaces. The contour of the coastline, for example a bay, will modify the nature of the wave front and this too will influence the behaviour of the horizontal field near the coastline. The horizontal extent of the structure can also have an important effect on the induced field. If the structure has a length of the order of half a wavelength, constructive interference can occur resulting in large enhancements of the induced field over the trailing edge, this being brought out by the dyke and sea mount models. In general, it is apparent that an irregular ocean bottom, or a large submerged structure, affects the induced fields at the surface only for rather shallow ocean depths (less than 40 m for a wavelength of approximately 360 m). Thus it appears that it may be feasible to use aerial measurements of ocean wave induced magnetic fields to detect shallow submerged structures such as reefs and sea mounts. To investigate deeply submerged structures, longer wavelengths would be required. A wavelength of 4×10^{4} m corresponds to a period of 160 seconds in an ocean of infinite depth, and such a wave should, by analogy, be useful for probing structures at depths up to four kilometers. (Evidence of induction effects by such long period waves has been found by Klein et al (1975) among others).

As pointed out by many authors, including Leibo et al (1975), the behaviour of the vertical component of the magnetic field should be quite different from the behaviour of the horizontal field, especially in situations where symmetry is not preserved in the horizontal direction. It would be of interest to extend this analogue technique to study the induced vertical component, in order to compare the behaviour of this component with the behaviour of the horizontal field. The models could also be extended to include a finitely conducting ocean bottom. A study of the induction effects for longer period ocean waves would be of value in probing to greater ocean depths, and a study of structures of different sizes would help separate interference effects from the geometrical effects. A magnetic field survey over some submerged structures in the ocean would be of interest, in order to provide a geophysical confirmation of the results obtained from the laboratory analogue model study.

REFERENCES

Barlow, W.H., 1849, On The Spontaneous Electric Currents Observed In The Wires Of The Electric Telegraph. Phil. Trans: 125-162

Beal, H.T. and Weaver, J.T., 1970. Calculation Of Magnetic Variations Induced By Internal Ocean Waves. Journal of Geophysical Research, 75(33):6848-6851

Coulson, C.A., 1955. Waves, Oliver and Boyd, Edinburgh, 159 pp

Crews, A. and Futterman, J., 1962. Geomagnetic Micro-pulsations Due To The Motion Of Ocean Waves. Journal of Geophysical Research, 67(1):299-306

Faraday, M., 1832. Experimental Researches in Electricity. Journal of the Royal Society, Phil. Trans:125-162

Ferraro, V.C. and Plumpton, C., 1961. Magneto-Fluid Mechanics. Oxford University Press, London, 181 pp

Gellibrand, H., 1635. A Discourse Mathematical On The Variations Of The Magnetic Needle, Together With Its Admirable Diminution Lately Discovered. W. Ionis, London

Gilbert, W., 1600 (Tr. 1851). De Magnete. Dover Publications Ltd., N.Y., 368 pp

Goldstein, H., 1950. Classical Mechanics. Addison-Wesley, Mass., 399 pp

Graham, G., 1724. An Account Of Observations Made Of The Variations Of The Horizontal Needle At London In The Latter Part Of The Year 1722 And Beginning Of 1723. Phil Trans:96-107

Groskaya, Ye. M, Skrynnikov, R.G., and Sokolov, G.V., 1972. Magnetic Field Variations Induced By The Motion Of Sea Waves In Shallow Water. Geomagnetism and Aeronomy, 12(1):131-134

Klein, M., Louvet, P., Morat, P., 1975. Measurement Of Electromagnetic Effects Generated By Swell. Physics of the Earth and Planetary Interiors 10:49-54

Larsen, J.C., 1971. The Electric Fields Of Long And Intermediate Water Waves. Journal Of Marine Research, 29:28-45

Leibo, A.B., Semenov, V.Yu, Fonarev, G.A., 1975. K Voprosu O Magnitnom Pole Ot Morskikh Voln. Geomatnitnie Issledovanie, 16:28-29

Longuet-Higgins, M.S., Stern, M.E., and Stommel, H., 1954. The Electric Field Induced By Ocean Currents And Waves With Applications To The Method Of Towed Electrodes. Papers In Physical Oceanography and Meteorology, 13(1):1-37

Maclure, K.C., Hafer, R.A., and Weaver, J.T., 1964. Magnetic Variations Produced By Ocean Swell. Pacific Naval Laboratory Technical Note, No. 64-8

Neckham, A., 1163. De Natura Rerum Libri Duo, Longman, London, 521 pp

Ng, T.P. and Dosso, H.W., 1970. Laboratory Simulation Of Magnetic Variations Associated With Ocean Waves And Swells. University of Victoria, Geophysics Report, 70-1

Podney, W., 1975. Electromagnetic Fields Generated By Ocean Waves. Journal of Geophysical Research, 80(21):2977-2990

Preisendorfer, R.W., Larsen, J.C., Sklarz, M.A., 1974. Electromagnetic Fields Induced By Plane-Parallel Internal And Surface Ocean Waves. Hawaii Institute Of Geophysics, Report No. HIG-74-8

Semonov, V. Yu. and Fonarev, G. A., 1975. O Zatykhanii V Atmosfere Magnitnovo Polya, Indutzirovannovo Morskimi Volnami. Geomagnetizm i Aeronomiya, 15(6):1127-1128

Warburton. F. and Caminiti, R., 1964. The Induced Magnetic Field of Sea Waves. Journal of Geophysical Research, 70(20):4311-4318

Weaver, J.T., 1965. Magnetic Variations Associated With Ocean Waves And Swell. Journal of Geophysical Research 70(8):1921-1929

Woods, R.G., 1965. Magnetic Variations Associated With Waves And Swell In A Shallow Sea. Pacific Naval Laboratory Technical Note, No.65-6

Young, F.B., Gerrard, H., and Jerons, W., 1920. On Electrical Disturbances Due To Tides And Waves. Philos. Mag., 40:149-159

APPENDIX A

Effect of Fluid Depth on the Model Linear Scale Factor

The linear scaling factor depends directly on the wavelength, as indicated by Eq (33). This dependence could be a problem in modelling experiments in that the wavelength changes (through Eq (35)), as the fluid depth changes, even when the frequency is held constant. A computer programme was written to evaluate Eq (33) for a fixed frequency of 4.0 Hz, taking into account the changes in wavelength (Eq (35)) due to changes in fluid depth. The results are shown in Fig. 7 for a model surface tension of .487 nt m^{-1}, a model fluid (mercury) conductivity of 1.04×10^6 S m^{-1}, and an ocean conductivity of 4.5 S m^{-1}. For the shallow fluid depth of d_1=.15 cm, the linear scaling factor is only 8% larger than the scale factor for the mercury depth of 2.8 cm, the largest depth used in the model study.

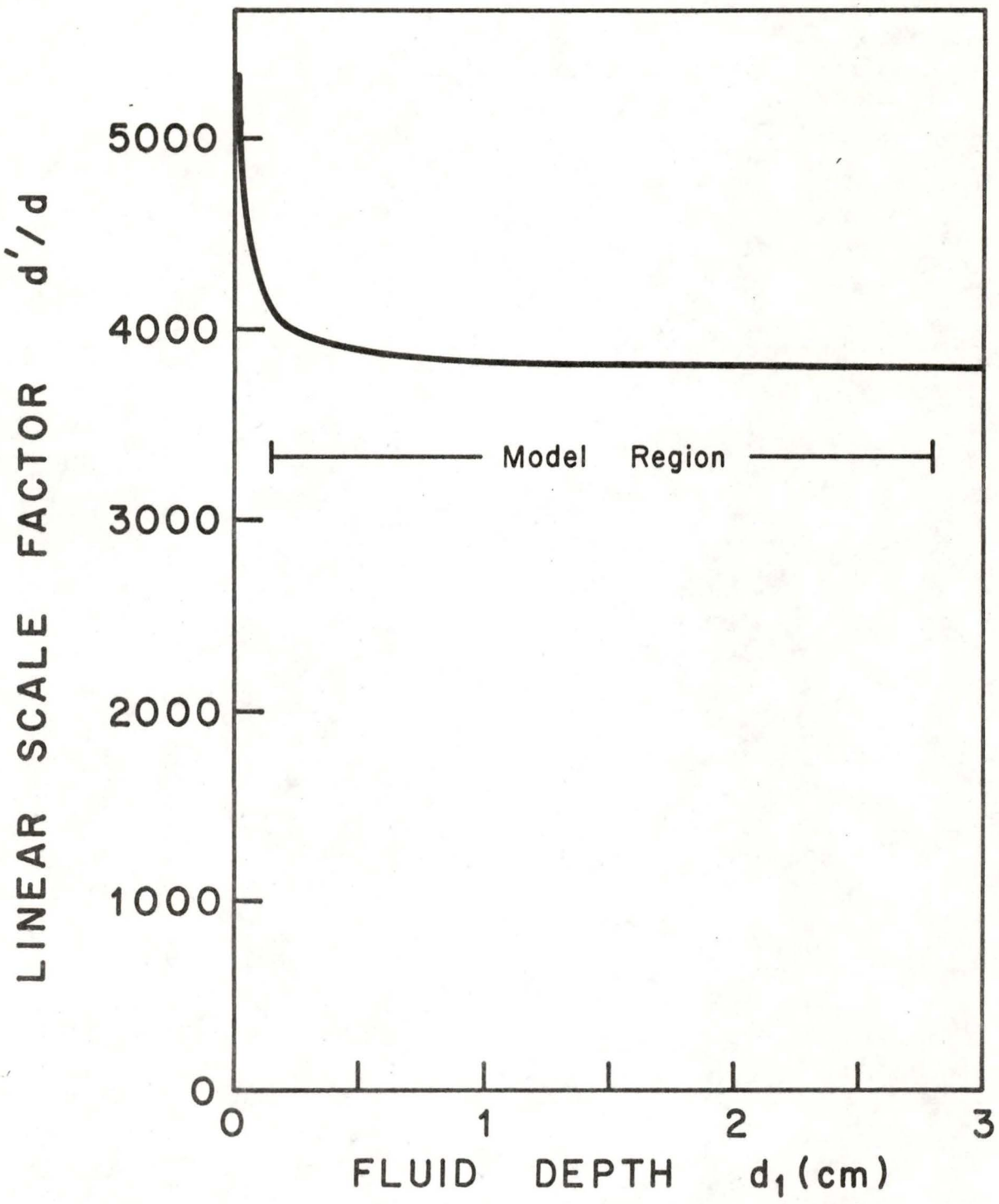

Fig. 7. Model linear scale factor (d'/d) as a function of fluid depth (d_1)

APPENDIX B

The Effect of Fluid Depth on the Wavelength and the Effect of Fluid Depth on the Induced Field

Equation (4) states that the induced field is a function of fluid depth, both directly, and through a dependence on the wave number k. To take into account the change in wave number with changing fluid depth, Eq (35) was used to calculate the wavelength for model fluid depths d<3 cm. Equation (4) was then used to compare the horizontal induced field for varying fluid depth (B_y) with the horizontal induced field for the standard fluid depth (B_{yr} at depth d=2.8 cm). The ratio B_y/B_{yr} as a function of fluid depth is shown in Fig. 9 for a model fluid (Hg) conductivity of 1.04×10^6 S m^{-1}, and a model frequency of 4.0 Hz. For the shallow fluid depth of d_1=.15 cm, the ratio B_y/B_{yr} has a value of .42, increasing rapidly as the fluid depth d_1 is increased. Since the induced field was less than the reference field for all model fluid depths, an enhancement above the reference field must be due to some phenomena involving non-uniformity of the structure.

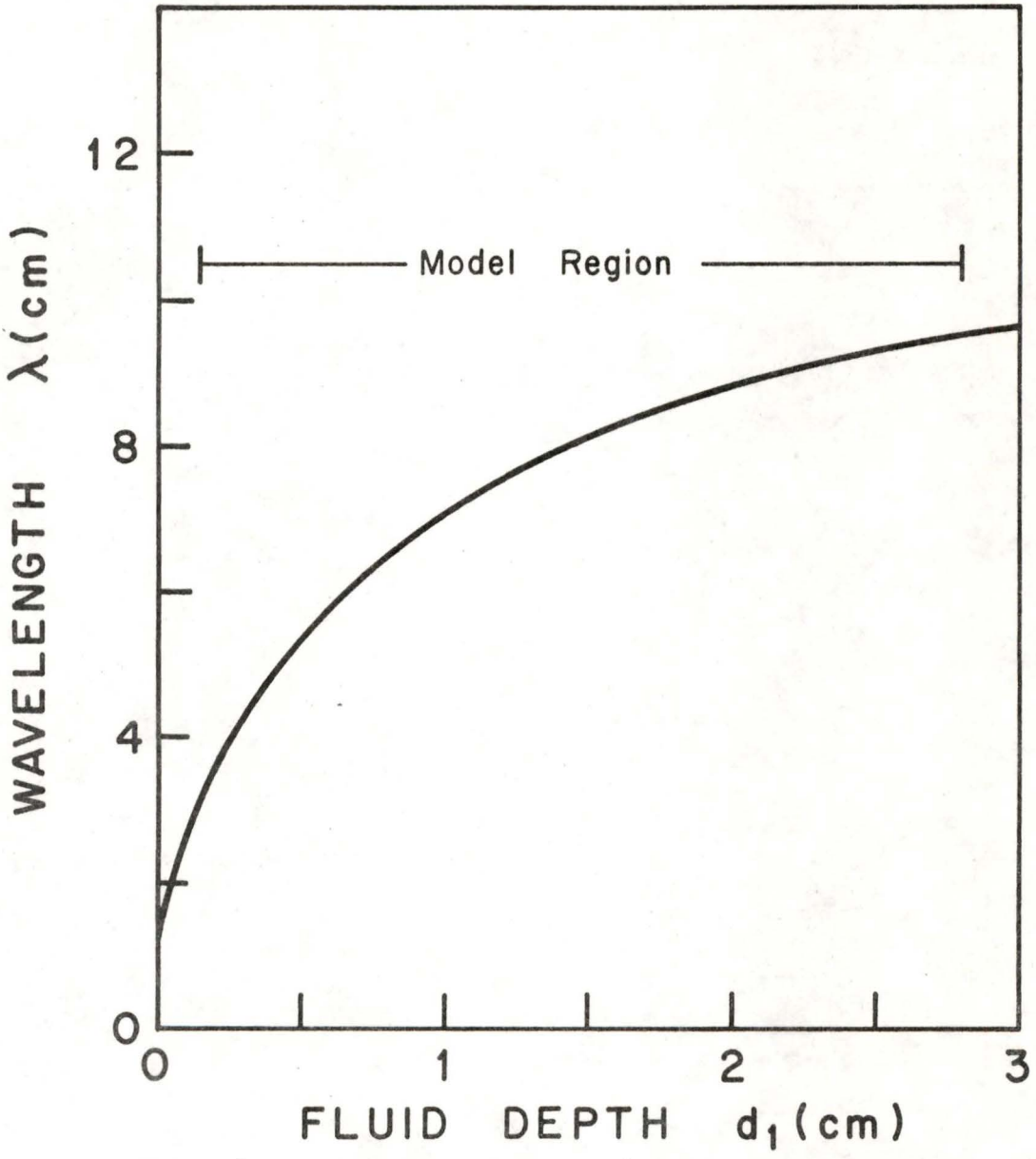

Fig. 8. Model Wavelength (λ) as a function of fluid depth (d_1)

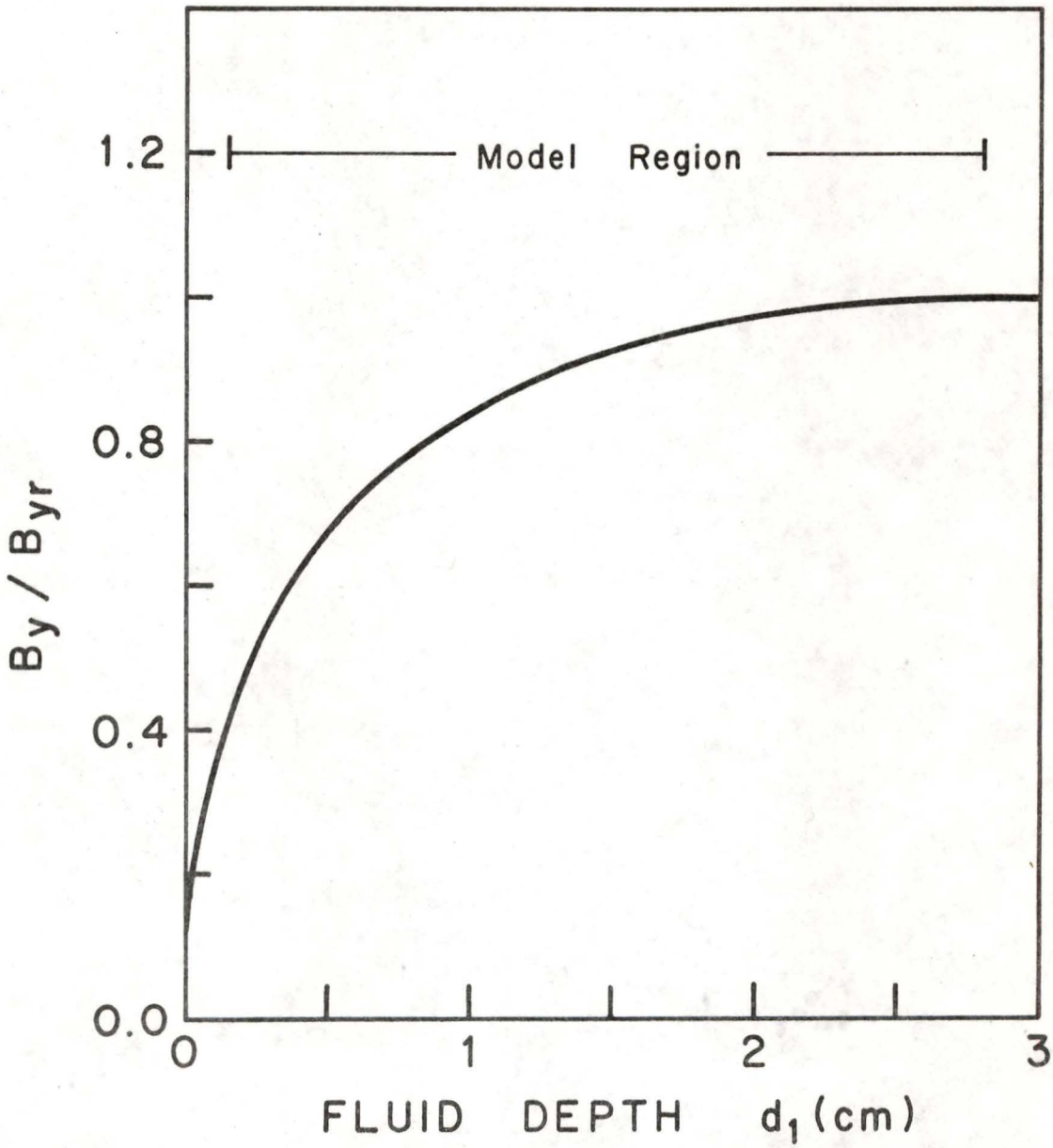

Fig. 9. Ratio of the induced horizontal magnetic field (B_y) for changing fluid depth (d_1) to the induced field (B_{yr}) for a fixed fluid depth of 2.8 cm (mercury)

VITA

Surname: MILES Given Names: TIMOTHY JOHN

Place of Birth: VICTORIA, B.C. Date of Birth: October 16, 54

Educational Institutions Attended, with Dates of Entering and Leaving:

UNIVERSITY OF VICTORIA, VICTORIA 1972 to 1976

UNIVERSITY OF VICTORIA, VICTORIA 1976 to 1978

_____ ____ to ____

_____ ____ to ____

Degrees, Diplomas, etc., Awarded, with Dates and Names of Institutions:

B. Sc. (Honours) 1976 University of Victoria, Victoria

_____ ____ _____

Honours and Awards:

_____

Publications:

Miles, T. and Dosso, H.W., 1977. An Analogue Model For Studying Magnetic Variations Induced By Ocean Waves. Physics of the Earth and Planetary Interiors, 14:137-142

Miles, T. and Dosso, H.W., 1978. An Analogue Model Study of Ocean-wave Induced Magnetic Field Variations Near a Coastline. Journal of Geomagnetism and Geoelectricity (in press)

PARTIAL COPYRIGHT LICENSE

I hereby grant the right to lend my thesis or dissertation (the title of which is shown below) to users of the University of Victoria Library, and to make single copies only for such users or in response to a request from the library of any other university, or similar institution, on its behalf or for one of its users. I further agree that permission for extensive copying of this thesis for scholarly purposes may be granted by me or a member of the University designated by me. It is understood that copying or publication of this thesis for financial gain shall not be allowed without my written permission.

Title of Thesis

A Laboratory Analogue Model Study of Magnetic Variations Induced by Ocean Waves

Author [redacted]

signature

T. Miles
name

March 29, 1978
date